JMEPEG (2017) 26:207–213
DOI: 10.1007/s11665-016-2436-2

1059-9495/$19.00

Modeling the Controlled Recrystallization of Particle-Containing Aluminum Alloys

Khaled Adam, Jameson M. Root, Zhengdong Long, and David P. Field

(Submitted June 2, 2016; in revised form October 14, 2016; published online December 1, 2016)

The recrystallized fraction for AA7050 during the solution heat treatment is highly dependent upon the history of deformation during thermomechanical processing. In this work, a state variable model was developed to predict the recrystallization volume fraction as a function of processing parameters. Particle stimulated nucleation (PSN) was observed as a dominant mechanism of recrystallization in AA7050. The mesoscale Monte Carlo Potts model was used to simulate the evolved microstructure during static recrystallization with the given recrystallization fraction determined already by the state variable model for AA7050 alloy. The spatial inhomogeneity of nucleation is obtained from the measurement of the actual second-phase particle distribution in the matrix identified using backscattered electron (BSE) imaging. The state variable model showed good fit with the experimental results, and the simulated microstructures were quantitatively comparable to the experimental results for the PSN recrystallized microstructure of 7050 aluminum alloy. It was also found that the volume fraction of recrystallization did not proceed as dictated by the Avrami equation in this alloy because of the presence of the growth inhibitors.

Keywords high strength aluminum alloy 7050AA, Monte Carlo Potts model, particle stimulated nucleation (PSN) of recrystallization, recrystallization, state variable model

1. Introduction

Recrystallization is an important consideration for industrial processing of aluminum alloys (Ref 1, 2). Controlling the microstructure and texture during recrystallization is essential to optimize the properties (Ref 3, 4). The recrystallization behavior of 7xxx aluminum alloys is dependent upon the particle size, spatial distribution, and the volume fraction in the matrix (Ref 6). During the production of 7050 aluminum alloys, decomposition and dissolution of constituent second-phase particles can take place at every stage of processing and, in turn, can influence the evolution of microstructure in the subsequent stages (Ref 5). During the solidification stage, insoluble constituent particles are colonized on the grain boundaries (Ref 7). These particles tend to be relatively large (on the order of microns) and interrupt the flow of metal during the hot rolling stage (Ref 2). Thus, the stored energy and stored energy gradient, which are regarded as the main drivers for nucleation of recrystallization, are expected to be high adjacent to coarse particles (Ref 8-10). There also tends to be a large texture gradient due to the tortuous flow of metal around these particles.

In this work, the distribution of stored energy is related to the hot rolling parameters and the gradient of the stored energy is related to the coarse particle distribution which can be determined from backscattered electron (BSE) images (Ref 3). The recrystallized nuclei form preferentially at positions of high stored energy and high orientation gradient (Ref 10). Also, the orientation of recrystallization nuclei in PSN regions tends to be almost randomly oriented with respect to the average polycrystalline sample orientation (Ref 11, 12).The addition of zirconium can form stable phases such as Al_3Zr during the homogenization stage, which tends to prevent the growth of recrystallized grains in the following stages (Ref 13-15). These Al_3Zr dispersoids are mainly found in the grain center and very slight in the near-grain-boundary regions (Ref 16).Therefore, recrystallization does not proceed as dictated by the Avrami equation in high-strength 7050 aluminum alloy.

AA7050 aluminum alloy is widely used in critical aircraft parts (such as wing ribs, spars, and fuselage frames) because it consolidates high strength, low density, stress-corrosion cracking resistance, and better fracture toughness than other 7xxx series alloys (Ref 17, 18). Microstructural modeling of thermomechanical processing is well documented as a useful technique for optimizing processing conditions in the metal industry. While some attempts have been made for aluminum alloys (Ref cf. 19), presently no successful model has been developed for predicting the evolved microstructure during the solution treatment of these 7xxx alloys.

Developing an adequate model that predicts the recrystallization fraction and simulates the evolving structure during thermomechanical processing is required (Ref 20). In the literature, the recrystallized fraction can be determined through an Avrami equation type as a function of annealing time (Ref 21). However, due to growth inhibitors, full recrystallization cannot be reached. It is of interest to predict the controlled recrystallization fraction by modifying the Avrami equation to take into account deformation conditions such as strain rate and deformation temperature (both are combined in the Zener-Hollomon parameter), and stored energy that results from hot deformation. The prediction of recrystallization behavior and microstructure evolution based on processing parameters of hot

Khaled Adam and **David P. Field**, School of Mechanical and Materials Engineering, Washington State University, Pullman, WA 99164; **Jameson M. Root**, School of Mechanical and Materials Engineering, Washington State University, Pullman, WA 99164, and School of Materials Engineering, Purdue University, West Lafayette, IN 47907; and **Zhengdong Long**, Kaiser Aluminum, Trentwood Works, Spokane Valley, WA 99216. Contact e-mail: k-adem@wsu.edu.

deformation processes has been addressed by several researchers (Ref 19, 22-25). The techniques that were used in these studies did not include the spatial inhomogeneity of recrystallization in a real microstructure, and they do not provide information on the morphology of the resultant recrystallized structure. On the other hand, computer simulations along with more accurate modeling of the evolving microstructure can provide this information (Ref 26-28). In this research, a state variable-based model has been coupled with the Monte Carlo Potts (MC) model to model the recrystallization volume fraction of the metal as a function of processing parameters. The spatial inhomogeneity of nucleation is obtained from measurement of the actual second-phase particle distribution in the matrix identified using backscattered electron (BSE) imaging. The initial microstructures for the simulations were obtained using electron backscatter diffraction (EBSD).

2. Experimental Details

7050 Al alloy strips were cut from the mid-thickness and mid-width section of a hot-rolled 50.8-mm (2 inch)-thick plate. The chemical composition of the AA7050 used in the present analysis in (wt.%) was 6.2% Zn, 2.3% Cu, 2.2% Mg, and 0.12% Zr with minor amounts of Si, Fe, Mn, Cr, and Ti. Cubically shaped samples $20 \times 15 \times 15$ mm^3 were cut from strips and machined to align with the original rolling and normal directions of the plate. SEM samples were ground and polished mechanically. Micro-hardness indentations were used as fiducial markers to determine precisely the regions for EBSD and BSE observations. High-resolution SEM was conducted in a field emission scanning electron microscope (FESEM) operated at 20 keV. EBSD was carried out with scans over square regions on the order of 4×10^6 μm^2. A representative EBSD data set was converted into a discretized matrix based on crystallographic orientation misorientation data (Ref 29). A custom FORTRAN code was used to incorporate low-angle misorientations within each grain. The ImageJ software package (Ref 30) was used to threshold the BSE images to determine the size distribution and area fraction of large particles (see Fig. 1). To minimize the effects of noise, all particles smaller than 4 pixels were ignored; this means that only particles with a diameter larger than 1 μm were included in the analysis. The EBSD and BSE measurements were taken primarily in the RD-ND plane to best capture the orientation gradients that exist in the structure, while token analyses were also performed on the other two mutually orthogonal plane sections. Figure 2(b) shows a typical BSE image with coarse particles as black spots in a white matrix. It is apparent that these large particles are distributed along the rolling direction, as quantified in a previous publication (Ref 3).

3. Description of the State Variable Recrystallization Model for AA7050

Recrystallization fractions of polycrystalline materials are often represented mathematically using an Avrami-type equation. We use the same approach herein, but due to the presence of growth inhibitors in this kind of alloy, full recrystallization cannot be reached without first dissolving the Zr-based pinning particles. Therefore, the Avrami equation is herein amended to represent the kinetics of recrystallization to a final recrystallization fraction less than 1. The fraction of recrystallized structure (f or $K_{\max}$) at a given recrystallization temperature is given by the revised Avrami equation (Eq 1). Figure 2 schematically represents the presumed recrystallization behavior in the 7050 aluminum alloy investigated as represented by this equation.

$$f = K_{\max}[1 - \exp(-b\tau^n)] \quad \text{(Eq 1)}$$

Including a number of judicious assumptions for developing a model to predict recrystallization fraction in a rolled particle-containing alloy is unavoidable. The essential assumptions include that: (i) The solute concentration is assumed constant in the matrix; (ii) the stored energy spatial distribution is related to

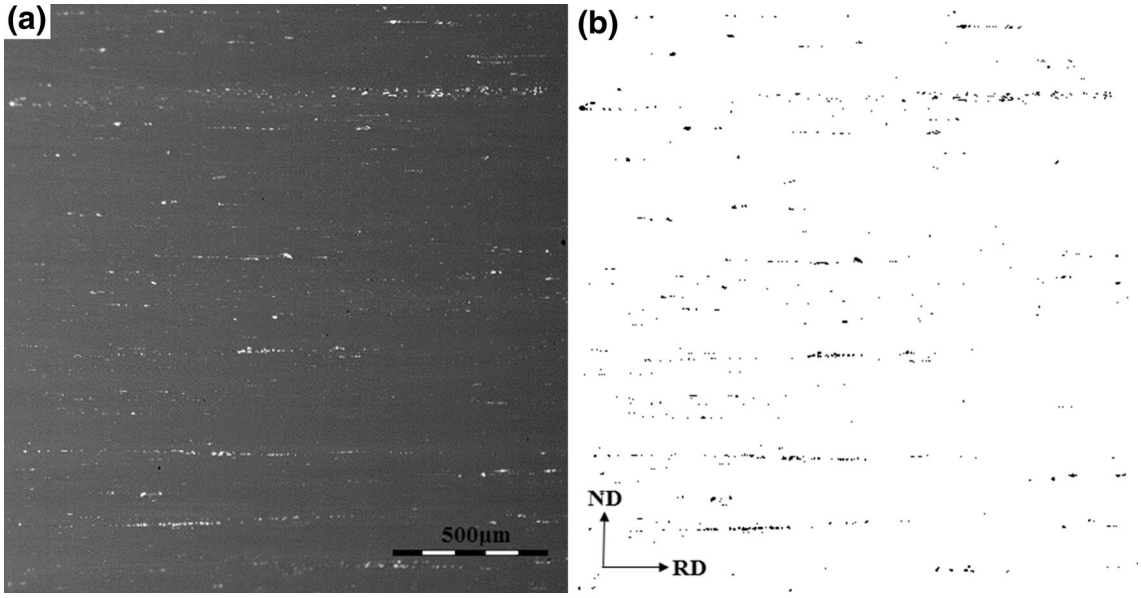

Fig. 1 (a) BSE image and (b) corresponding binarized image showing the representative particle distribution in the rolled AA 7050 structure (The magnification bar is 500 μm)

the spatial distribution of coarse particles in the matrix; (iii) the texture and grain boundary effects are uniform; and (iv) recrystallization is a function of composition, but all experiments were performed on specimens from $t/2$ so the composition is assumed to be uniform.

In hot rolling, the stored energy, strain rate, and temperature in the metal are fluctuating constantly as a function of time and position (Ref 22). An accurate prediction of microstructural evolution and recrystallization behavior of aluminum alloys is highly dependent upon the history of deformation during thermomechanical processing (Ref 31). A number of deformation experiments on ingot samples of 7050 were performed at elevated temperature using plane strain deformation so as to simulate hot rolling conditions (Ref 32). It will be demonstrated that the static recrystallization kinetics of high-strength aluminum alloys after hot rolling can be effectively described by three parameters: temperature-compensated strain rate (Zener-Hollomon parameter, Z), recrystallization temperature T_{rex}, and accumulated stored energy S.

$$K_{\max} = K_0(Z, T_{\text{rex}}, S) \qquad \text{(Eq 2)}$$

A model describing the relationship between these parameters and the fraction recrystallized was developed as part of this work (see the "Appendix"). Figure 3 shows the recrystallization fraction that was predicted by the state variable model and measured experimentally for AA7050 at a recrystallization temperature of 470 °C (i.e., the solutionizing temperature). Each point represents the experimental and modeled recrystallization fractions after a given set of deformation conditions and a given annealing time. Perfect agreement between the model

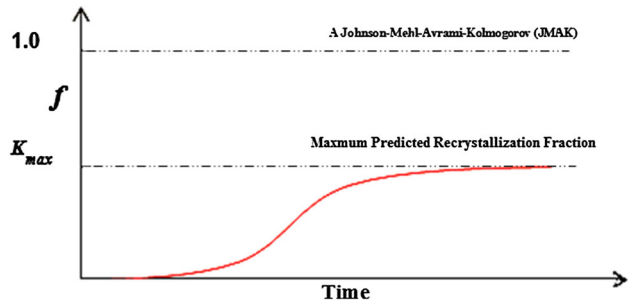

Fig. 2 Schematic of the assumed recrystallization kinetics in high-strength 7050 Al alloy

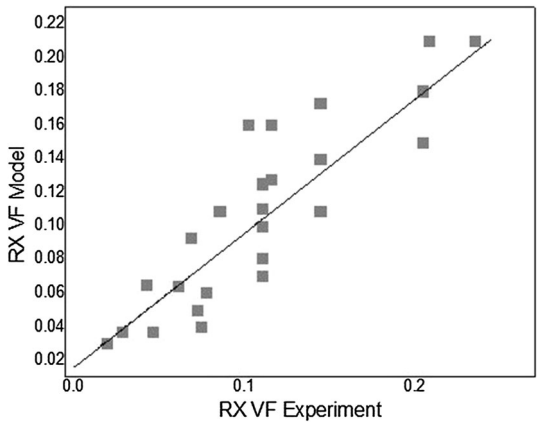

Fig. 3 Diagram shows the recrystallization fraction predicted by state variable model compared with the experiment results for a 7050 Al alloy

and experiment would be achieved for all points lying on the dashed line. The reasonable consistency between model predictions and experimental results is an indication that the recrystallization behavior of hot deformation is influenced by the identified variables mentioned above.

In addition to the state variable model that retrieves stored energy, a platform for describing the spatial dependence of structural evolution is required. A mesoscale model exhibiting the microstructural evolution over a two-dimensional spatial grid is used for this purpose. The following section presents a brief description of the Monte Carlo Potts model.

4. Simulation Approach

4.1 Monte Carlo Model

In the current work, computer simulation of the recrystallization process was undertaken using a Monte Carlo Potts model. The initial microstructure used as input for MC simulation originated from the EBSD data using a domain size of 274 × 268 sites. Every lattice site embedded in a grain was allocated with an index $\boldsymbol{S_i}$ referring to the crystallographic orientation (spin) of that grain. Lattice sites surrounded by sites of different crystallographic orientations were considered as being located at a grain boundary, whereas lattice sites that were neighbored by sites with the same orientations were regarded as being embedded in grain interiors (Ref 33). Also, the stored energy resulting from deformation can be assigned to every lattice site. Therefore, every site has an associated stored energy $\boldsymbol{H}(\boldsymbol{s_i})$ that contributes to the total energy of the system. The stored energy was set to be a positive arbitrary value varied from 1 to 10 (with 10 having the highest stored energy) for lattice sites belonging to the particle deformation zones. The total system energy is described by the Hamiltonian as given in the following equation:

$$E = J/2\sum_{i=1}^{N}\sum_{j=1}^{NN}\left(1-\delta\left(S_i, S_j\right)\right) + \sum_{i} H(S_i) \qquad \text{(Eq 3)}$$

The evolution of the structure is modeled by choosing a site from the recrystallized orientation set and a new orientation at random from the set of allowable values. The total system energy change, ΔE, for changing the site to the new orientation is calculated, and the flipping is executed with a transition probability P, such that (Ref 34)

$$P(\Delta E, T) = \begin{cases} 1 & \Delta E \le 0 \\ \exp\left(-\frac{\Delta E}{KT}\right) & \Delta E > 0 \end{cases} \qquad \text{(Eq 4)}$$

Each dissimilar pair of nearest neighbor points contributes a unit of grain boundary energy J to the system. In simulation of recrystallization, the stored energy per site is presumed to be positive at time zero for the deformed matrix and zero for the recrystallized matrix (Ref 35). The external sum i is a summation over all N sites in the system, whereas the inner sum j is over nearest neighbors (NN) only. $\boldsymbol{S_i}$ and $\boldsymbol{S_j}$ are old and new (randomly selected) lattice orientations, respectively, $\boldsymbol{K}$ is the Boltzmann constant, and $\boldsymbol{T}$ is the absolute temperature. Unlike the physical temperature, the temperature in the context of the Monte Carlo model governs the degree of disorder in the lattice. The lattice temperature ($\boldsymbol{kT}$) is mostly set to 0.2-0.3 in order to maintain boundary roughness and to avoid lattice

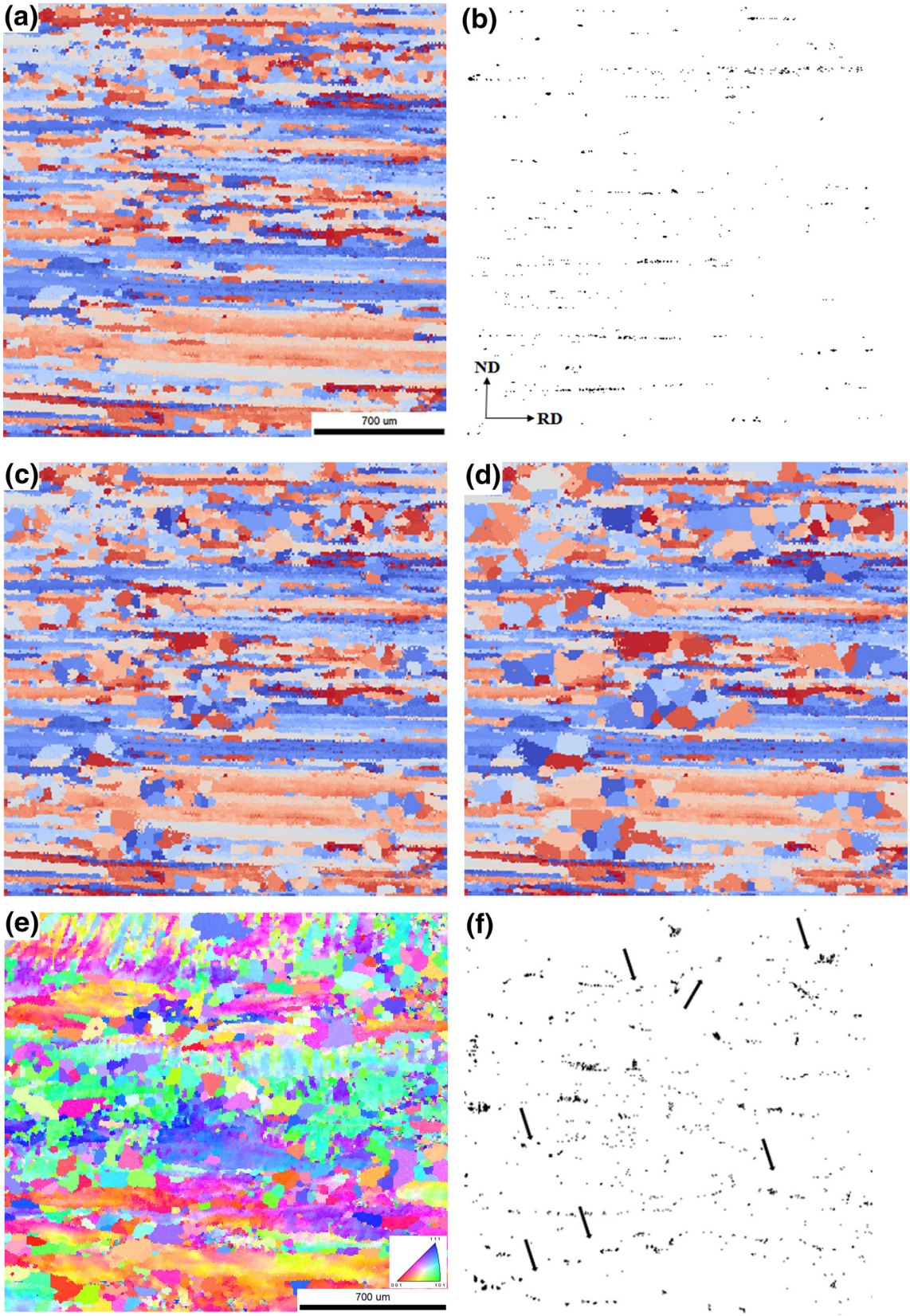

Fig. 4 Snapshots for microstructural evolution using Monte Carlo Potts model (a, b) initial real 7050 Al alloy microstructure along with real thresholded BSE image, (c) 16.8% recrystallization fraction (15 MCST), (d) 29% recrystallization fraction (~40 through 100 MCST), (e, f) a microstructure of recrystallized grain in alignment with large particle distribution (the magnification bar is 700 μm)

pinning effects (Ref 36). One Monte Carlo time step (1 MCS) is defined as N reorientations where each of the N sites is given an opportunity to change orientation. The range of orientation values can be split into recrystallized and non-recrystallized sets. The orientations of the recrystallization nuclei are taken from the texture near particles and are observed to be almost random. The simulation was carried out with site saturated surface nucleation, which means that all nuclei were injected into the matrix with a unique orientation value distributed spatially according to the particle distribution in the BSE images.

5. Results and Discussion

5.1 Microstructure Evolution

Figure 4(a) and (b) shows the initial hot-rolled microstructure including low-angle misorientations within each grain for high-strength aluminum alloy 7050 and binarized BSE images for the RD-ND plane. The black spots in the BSE image represent coarse particles that determine the regions of nucleation in the matrix. These Fe- or Si-based non-deformable particles affect the microstructure and texture during hot rolling by producing large deformation heterogeneities around the coarse particles (i.e., high stored energy). The recrystallization behavior is controlled by total stored energy and its spatial distribution in the matrix (Ref 23). These deformation heterogeneities are called particle deformation zones (PDZ) and often elongated in the direction of deformation. PDZ regions can act as the preferred sites for nucleation of recrystallized grains during subsequent treatment (Ref 10). In regions of particle clustering, the particle deformation zones overlap. Numerous sub-grains with random orientations in the particle-matrix interface are generated (Ref 37).

Due to the particle size and the degree of deformation (reduction 90%) which increases the stored energy during deformation, few recrystallized sub-grains were visible in the initial microstructure, shown in Fig. 4(a) and (b). In this research, a number of nuclei were added to the microstructure at simulation time zero (site saturation nucleation) (Ref 35) and distributed according to the particle distribution in the BSE thresholded images over the old recrystallized sub-grains. The recrystallized grains grow and migrate in longitudinal patterns parallel to the rolling direction in conjunction with the coarse particle distribution. These nuclei were growing in competition with each other similar to grain growth in a single-phase alloy. The mobility and migration of the new strain-free grains were isotropic; therefore, equiaxed polyhedra were expected in the recrystallized structure. Figure 4(c) and (d) shows the simulated evolved microstructure for the hot-rolled 7050 aluminum alloy. It was assumed that the recrystallized grains are completely strain-free with unique orientations and no observed angle misorientation. The recrystallized grains grow around the large particle into the deformed matrix in particle deformation zone domains. Generally, by comparing the spatial distribution of recrystallized grains in the EBSD images with coarse particles in BSE images, the conclusion that recrystallization has occurred mainly by the particle stimulated nucleation (PSN) mechanism is supported. Qualitatively, the simulated microstructures were in agreement with the experimental results for recrystallized microstructure of 7050 aluminum alloy.

Figure 4(e) and (f) shows the actual distribution of recrystallized grains within the AA7050 alloy. The black arrows point to locations of clustered recrystallized grains in the EBSD image and to large non-deformable particles in the binarized BSE image. This demonstrates that recrystallized grains are not randomly distributed and again confirms that PSN is the primary mechanism for nucleation of recrystallized grains in AA7050. The recrystallized grains tend to gather around the coarse particles in arrays parallel to the rolling direction (Ref 38).

5.2 PSN Recrystallization Behavior During Simulation

Figure 5 shows the typical sigmoidal form of the recrystallization kinetics which characterizes the simulation results very well. The plot shows that a finite recrystallized nuclei fraction was assigned at time zero, followed by a rapid increase in the recrystallization rate (linear slope), and lastly due to impingement of growing grains and a matrix containing recrystallization-resistant particles; a declining rate of recrystallization is noticed as well. The recrystallized fraction is about 29 percent for this simulation, which was determined by the state variable model for a strain rate = 2.3/s, deformation temperature = 385 °C, and solution heat treatment temperature = 470 °C to a final rolling reduction of 0.90.

PSN recrystallization typically initiates at many nuclei; therefore, a large quantity of recrystallized sub-grains were inserted within the particle-affected zones in the matrix. Some of these grains will grow, while others shrink with time, and the average number of recrystallized grains will drop during recrystallization (Ref 39). Figure 6 shows the decline in the number of recrystallized grains against recrystallization fraction (RXF) at early simulation times (namely 0-40 MCS time). This is because the growth rate of recrystallized grains was driven by stored energy in the early stages of simulation. This growth rate declined when the stored energy was consumed in the particle deformation zones (after 40 MCS time). Figure 6 shows the decline in the number of recrystallized grains against the recrystallization fraction (RXF) at early simulation times (namely 0-40 MCS time). This is because the growth rate of recrystallized grains was driven by stored energy in the early stages of simulation. This growth rate declined when the stored energy was consumed in the particle deformation zones (after

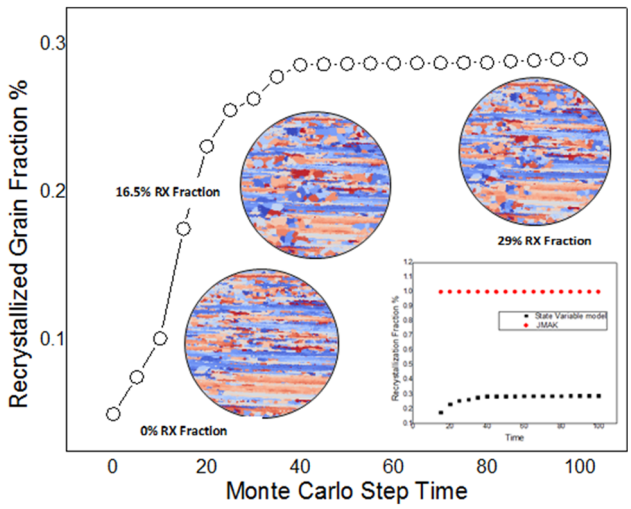

Fig. 5 Recrystallization kinetics obtained from Monte Carlo simulation result

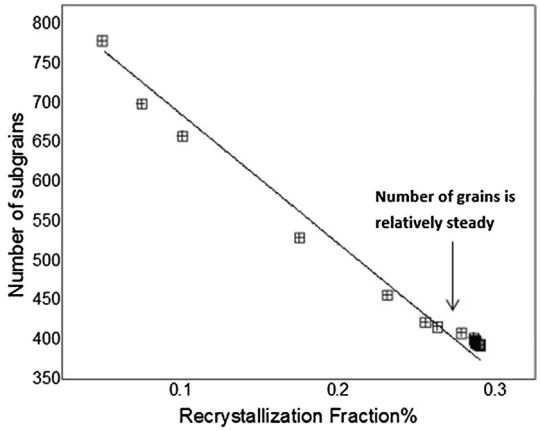

Fig. 6 Drops in the recrystallized sub-grains number vs. RX fraction as determined by the Monte Carlo Potts model

40 MCS time), and the recrystallizing grains no longer had the driving force to overcome the recrystallization-resistant matrix. After that time, a small variation in recrystallization volume fraction appeared that can be attributed to the growth of grains under the driving pressures of the recrystallized grain boundaries. However, the recrystallized grains were constrained by impingement with unrecrystallized grains previously assigned with low stored energy outside of the particle deformation zone where the effect of dispersoids (Al_3Zr) is enough to overcome the driving force for boundary migration and recrystallization will be halted (Ref 40). Thus, the PSN nuclei are not able to grow out of the deformation zone (Ref 41).

6. Summary and Conclusion

The present work shows an obvious link between the deformation conditions and the static microstructural evolution. The recrystallized fraction for AA7050 during the solution heat treatment is highly dependent upon the history of deformation during thermomechanical processing. A Monte Carlo Potts model has been used to simulate the evolved microstructure during static recrystallization with the given recrystallization fraction determined already by the state variable model for AA7050 alloy. The state variable model showed good fit with the experimental results. The recrystallization behavior in this alloy was dominated by particle stimulated nucleation. The realistic particle distributions of second-phase particles along with a deformed microstructure were incorporated into the Potts model as the initial point for simulation of the microstructure. The recrystallization behavior is highly affected by stored energy around the coarse particles in the early stages of simulation; the growth of recrystallized grains progresses rapidly, but becomes inhibited once the high-energy particle deformation zone was consumed. The simulated microstructures are quantitatively comparable to the experimental results for the recrystallized microstructure of 7050 aluminum alloy. The recrystallized grains tend to cluster around the coarse particles in arrays parallel to the rolling direction. This demonstrates that recrystallized grains are not randomly distributed and PSN is considered as the primary mechanism for nucleation of recrystallized grains in AA7050. The average number of recrystallized grains drops during grain growth due to a ripening procedure.

Acknowledgments

The authors certify that there is no actual or potential conflict of interest in relation to this article.

Appendix

In the hot rolling stage of high-strength aluminum alloys, recovery and perhaps some recrystallization can take place between stands in a rolling mill. Therefore, it is presumed that deformation goes to increase dislocation density, but immediately after unloading as result of the deformation temperatures, recovery begins to take place. These events continually influence the stored energy rate in hot deformation. As stated in section 3 (Eq 1 and 2), the assumption is that the recrystallization kinetics follow a law similar to that proposed by Johnson, Mehl, Avrami, and Kolmogorov with the exception that complete recrystallization will not take place. In this state variable model, developed specifically for this study, the total fraction of recrystallization is equal to K_o, where

$$K_0 = B_1\left(\frac{S}{S_C}\right)^m [\tanh(C_1 \ln(1+Z))]^{m_1}\left(\frac{T_{\text{rex}}}{T_m}\right)^{n_1} \quad \text{(Eq 5)}$$

T_{rex} is the recrystallization temperature which is an external variable, while Z is the Zener-Hollomon parameter, S is stored energy and is an internal state variable that tracks evolution of the structure during deformation and annealing, and T_m is the melting temperature.

$$Z = \dot{\varepsilon}\exp\left(\frac{Q}{RT_{\text{def}}}\right) \quad \text{(Eq 6)}$$

$$S_c = 1000 \quad \text{(Eq 7)}$$

S_c is an arbitrary value representing the highest possible value for stored energy in the metal at any condition.

During hot deformation, the stored energy evolves following the relationship:

$$\dot{S} = C(Z)\dot{\varepsilon}\left[1 - \frac{S}{S_{\max}(Z)}\right] \quad \text{(Eq 8)}$$

where

$$C(Z) = B_3[\ln(Z+1)]^{m_3} \quad \text{(Eq 9)}$$

And the maximum equilibrium stored energy attainable at any given Z value is:

$$S_{\max} = S_c[\tanh(B_4 \ln(Z+1))] \quad \text{(Eq 10)}$$

Constants determined from experimental measurements of recrystallization at various deformation and annealing conditions were determined as follows: m = 0.48, B_1 =2.12, B_3 = 0.015 (fixed), m_3= 3.9, B_4= 0.79, C_1= 0.03 (fixed), Q = 50000 JK/mole (not a fitting parameter), R = 8.314 J/mole (not a fitting parameter), and with the initial condition, S (0) = 1 for hot-deformed AA7050 at a position in the center of the plate (t/2).

References

1. F.J. Humphreys and M. Hatherly, *Recrystallization and Related Annealing Phenomena, Chap. 15*, Elsevier Science Inc., Oxford, 1995
2. X. Song and M. Rettenmayr, Modeling Recrystallization in a Material Containing Fine and Coarse Particles, *Comput. Mater. Sci.*, 2007, **40**(2), p 234–245
3. D.P. Field, L. Behrens, and J.M. Root, Identification of Particle Stimulated Nucleation during Recrystallization of AA 7050, *Comput. Mater. Continua*, 2009, **14**(3), p 171–183
4. C.M. Sellars, Modelling Microstructural Development During Hot Rolling, *Mater. Sci. Technol.*, 1990, **6**, p 1072–1081
5. I.J. Polmear, *Light Alloys from Traditional Alloys to Nanocrystals*, Elsevier, Oxford, 2006
6. D. Dumont, A. Deschamps, and Y. Brechet, On the Relationship Between Microstructure, Strength and Toughness in AA7050 Aluminum Alloy, *Mater. Sci. Eng. A*, 2003, **1–2**(365), p 326–336
7. G. Totten and D.S. Mackenzie, *Handbook of Aluminum: Physical Metallurgy and Processes*, CRC Press LLC, Boca Raton, 2003
8. B. Radhakrishnan and G.B. Sarma, *Continuum Scale Simulation of Engineering Materials Fundamentals—Microstructures—Process Applications, Chap. 15*, WILEY-VCH Verlag GmbH & Co. KGaA, Weinheim, 2004
9. B. Radhakrishnany and G. Sarma, The Effect of Coarse Non-deformable Particles on the Deformation and Static Recrystallization of Aluminum Alloys, *Philos. Mag.*, 2004, **84**(22), p 2341–2366
10. R.D. Doherty and D.A. Hughes, Current Issues in Recrystallization: A Review, *Mater. Sci. Eng.*, 1997, **238**, p 219–274
11. O. Engler, Influence of Particle Stimulated Nucleation on the Recrystallization Textures in Cold Deformed Al-Alloys Part II—Modeling Of Recrystallization Textures, *Scr. Mater.*, 1997, **37**, p 1675–1683
12. B. Verlinden, J. Driver, I. Samajdar, R.D. Doherty, and R.W. Cahn, *Thermo-Mechanical Processing of Metallic Materials, Chap. 8*, Elsevier, Amsterdam, 2007
13. H. Weiland and S.W. Cheong, The Role of Zirconium Additions in Recrystallization of Aluminum Alloys, *Mater. Sci. Forum*, 2007, **558–559**, p 383–387
14. J.D. Robson and P.B. Prangnell, Dispersoid Precipitation and Process Modelling in Zirconium Containing Commercial Aluminum Alloys, *Acta Mater.*, 2001, **49**, p 599–613
15. Y.W. Riddle and T.H. Sanders, Recrystallization Performance of AA 7050 Varied with Sc and Zr, *Mater. Sci. Forum*, 2000, **331–337**, p 799–804
16. A.Z. Eivani, J. Zhou, and J. Duszczyk, *Recent Trends in Processing and Degradation of Aluminum Alloys*, Chap. 20, InTech., 2011
17. J.D. Robson, Microstructure Evolution in Aluminum Alloy 7050 during Processing, *Mater. Sci. Eng.*, 2004, **382**, p 112–121
18. J.T. Staley and D.J. Lege, Advances in Aluminum Alloy Products for Structural Applications in Transportation, *Journal De Physique IV*, 1993, **3**, p 179–190
19. H.E. Vatne and E. Nes, A Model for Recrystallization Kinetics, Texture and Grain Size Applied to Multipass Hot Rolling of an AlMgMn Aluminum Alloy, *Comput. Mater. Sci.*, 1996, **7**(1–2), p 5–10
20. D. Duly, G.J. Baxter, H.R. Shercliff, J.A. Whiteman, C.M. Sellars, and M.F. Ashby, Microstructure and Local Crystallographic Evolution in an Al-1 Wt% Mg Alloy Deformed at Intermediate Temperature and High Strain-Rate, *Acta Mater.*, 1996, **44**(7), p 2947–2962
21. M. Avrami, Kinetics of Phase Change I. General Theory, *J. Chem. Phys.*, 1939, **7**, p 1103–1112
22. H.E. Vatne, S. Benum, D. Ole, and E. Nes, The Effect of Particles on Recrystallization Textures and Microstructures, *Textures Microstruct.*, 1996, **26**, p 385–412
23. C.M. Sellars and Q. Zhu, Microstructural Modelling of Aluminum Alloys During Thermomechanical Processing, *Mater. Sci. Eng.*, 2000, **280**(1), p 1–7
24. H.E. Vatne, T. Furu, R. Ørsund, and E. Nes, Modelling Recrystallization After Hot Deformation of Aluminum, *Acta Mater.*, 1996, **44**(11), p 4463–4473
25. J.H. Beynon and C.M. Sellars, Modelling Microstructure and Its Effects during Multipass Hot Rolling, *ISIJ Int.*, 1992, **32**(3), p 359–367
26. F.J. Humphreys, Modelling Microstructural Evolution During Annealing, *Model. Simul. Mater. Sci. Eng.*, 2000, **8**(6), p 893–910
27. K. Marthinsen, J.M. Fridy, T.N. Rouns, K.B. Lippert, and E. Nes, Characterization of 3-D Particle Distributions and Effects on Recrystallization Kinetics and Microstructure, *Scr. Mater.*, 1998, **39**(9), p 1177–1183
28. P. Sepehrband and S. Esmaeili, A Methodology for Monte Carlo Simulation of Recrystallization in an Overaged and Cold-Rolled Precipitation-Hardenable Aluminum Alloy, *Scr. Mater.*, 2010, **63**, p 4–7
29. M.A. Groeber and M.A. Jackson, DREAM.3D: A Digital Representation Environment for the Analysis of Microstructure in 3D, *Integrating Mater. Manuf. Innov.*, 2014, **3**, p 5
30. M.D. Abramoff, P.J. Magalhaes, and S.J. Ram, Image Processing with ImageJ, *Biophotonics Int.*, 2004, **11**(7), p 36–42
31. T. Furu, H.R. Shercliff, G.J. Baxter, and C.M. Sellars, The Influence of Transient Deformation Conditions on Recrystallization During Thermomechanical Processing of an Al–1% Mg Alloy, *Acta Mater.*, 1999, **47**(8), p 2377–2389
32. J.M.M. Root, *Structure Evolution and Recrystallization in 7XXX Series Aluminum Alloys*, Washington State U, Pullman, 2010
33. E.A. Holm and C.C. Battaile, The Computer Simulation of Microstructural Evolution, *JOM*, 2001, **53**(9), p 20–23
34. M. Miodownik, *Computational Materials Engineering an Introduction to Microstructure Evolution, Chap. 3*, Elsevier, Oxford, 2007
35. A.D. Rollett and P. Manohar, *Continuum Scale Simulation of Engineering Materials Fundamentals—Microstructures—Process Applications, Chap. 4*, WILEY-VCH Verlag GmbH & Co. KGaA, Weinheim, 2004
36. K. Okuda and A.D. Rollett, Monte Carlo Simulation of Elongated Recrystallized Grains in Steels, *Comput. Mater. Sci.*, 2005, **34**, p 264–273
37. V. Marx, D. Raabe, O. Engler, and G. Gottstein, Simulation of the Texture Evolution During Annealing of Cold Rolled Bcc and FCC Metals Using a Cellular Automation Approach, *Textures Microstruct.*, 1997, **28**, p 211–218
38. R.A. Vandermeer and D.J. Jensen, Recrystallization in Hot vs Cold Deformed Commercial Aluminum: A Microstructure Path Comparison, *Acta Mater.*, 2003, **51**, p 3005–3018
39. G. Gottstein and L.S. Shvindlerman, *Grain Boundary Migration in Metals: Thermodynamics, Kinetics, Applications*, CRC Press Taylor & Francis Group, Boca Raton, 2010
40. L. Wu, W. Wang, Y. Hsu, and S. Trong, Effects of Homogenization Treatment on Recrystallization Behavior and Dispersoid Distribution in an Al–Zn–Mg–Sc–Zr Alloy, *J. Alloys Compd.*, 2008, **456**, p 163–169
41. O. Daaland and E. Nes, Recrystallization Texture Development in Commercial Al-Mn-Mg Alloys, *Acta Mater.*, 1996, **44**(4), p 1413–1435